

# Highly Dense and Perfectly Aligned Single-Walled Carbon Nanotubes Fabricated by Diamond Wire Drawing Dies

Guangtong Liu,<sup>†,‡,||</sup> Yuanchun Zhao,<sup>†,‡,⊥</sup> Ke Deng,<sup>‡</sup> Zheng Liu,<sup>‡,⊥</sup> Weiguo Chu,<sup>‡</sup> Jingran Chen,<sup>§</sup> Yanlian Yang,<sup>‡</sup> Kaihong Zheng,<sup>‡,⊥</sup> Haibo Huang,<sup>‡,⊥</sup> Wenjun Ma,<sup>§,⊥</sup> Li Song,<sup>§</sup> Haifang Yang,<sup>§</sup> Changzhi Gu,<sup>§</sup> Guanghui Rao,<sup>§</sup> Chen Wang,<sup>‡</sup> Sishen Xie,<sup>\*,§</sup> and Lianfeng Sun<sup>\*,‡</sup>

National Center for Nanoscience and Technology, Beijing 100080, China, Beijing National Laboratory for Condensed Matter Physics, Institute of Physics, Beijing 100080, China, Institute of Theoretical Physics, Chinese Academy of Sciences, Beijing 100080, China, and Graduate School of Chinese Academy of Sciences, Beijing 100049, China

Received November 18, 2007; Revised Manuscript Received February 3, 2008

## ABSTRACT

We have developed a low-cost and effective method to align single-walled carbon nanotubes (SWNTs) using a series of diamond wire drawing dies. The obtained SWNTs are highly dense and perfectly aligned. X-ray diffraction (XRD) indicates that the highly dense and perfectly aligned SWNTs (HDP-SWNTs) form a two-dimensional triangular lattice with a lattice constant of 19.62 Å. We observe a sharp (002) reflection in the XRD pattern, which should be ascribed to an intertube spacing 3.39 Å of adjacent SWNTs. Raman spectra reveal that the radical breath mode (RBM) of SWNTs with larger diameter in the HDP-SWNTs is suppressed compared with that of as-grown SWNTs. The HDP-SWNTs have a large density,  $\sim 1.09$  g/cm<sup>3</sup>, and a low resistivity,  $\sim 2$  mΩ cm, at room temperature, as well as a large response to light illumination.

Single-walled carbon nanotubes (SWNTs) have received intensified interest due to their potential applications in nanoscale materials and devices since their discovery.<sup>1</sup> To date, much effort has been devoted to fabricating large uniform and ordered nano- and microstructures of carbon nanotubes. Meanwhile, bulk materials of SWNTs also attract particular attention. As we know, the most interesting properties of carbon fullerenes appear in their condensed form.<sup>2-4</sup> Theoretical work predicts that this may also be true for carbon nanotubes.<sup>5-7</sup> However, SWNTs are usually entangled and poorly ordered by usual growth methods of arc discharge,<sup>8</sup> laser ablation,<sup>9</sup> or chemical vapor deposition.<sup>10</sup> Recently, a densely packed SWNT array (SWNT solid)<sup>11</sup> has been achieved by exploiting a liquid-induced collapse of SWNT forests,<sup>12</sup> while high-performance fibers<sup>13</sup> were obtained by directly spinning of carbon nanotube fibers.<sup>14</sup>

For these two materials, even a peak of (002) was observed in the X-ray diffraction (XRD) pattern, there is significant diffuse intensity at angles below the (002) peak. This indicates that some of the interlayer spacings are greater than that typical of graphene stacks. In this Letter, we reported a low-cost and effective method to align SWNTs using a series of diamond wire drawing dies. It is found that SWNTs can form crystalline structure by van der Waals force when they are perfectly aligned and ideally densely packed. XRD shows that these nanotubes form a two-dimensional triangular lattice with a lattice constant of 19.62 Å. Most interestingly, we observe a sharp (002) reflection arising from an intertube spacing of 3.39 Å for adjacent SWNTs, which is unobservable for individual SWNTs or small crystalline ropes of SWNTs.<sup>8,9</sup> In contrast to the as-grown SWNTs, the radical breath mode (RBM) of SWNTs with larger diameter in highly dense and perfectly aligned SWNTs (HDP-SWNTs) is notably suppressed.

The SWNTs used in this work were grown by floating catalytic chemical vapor deposition (CVD).<sup>15</sup> Under optimal growth conditions, the average diameter of individual SWNTs is  $\sim 16.0$  Å (see Supporting Information, Figure S1).

\* Corresponding authors. E-mail: slf@nanocr.cn (L.F.S.) and sxxie@aphy.iphy.ac.cn (S.S.X.).

<sup>†</sup> These authors contributed equally to this work.

<sup>‡</sup> National Center for Nanoscience and Technology.

<sup>||</sup> Institute of Theoretical Physics, Chinese Academy of Sciences.

<sup>⊥</sup> Graduate School of Chinese Academy of Sciences.

<sup>§</sup> Beijing National Laboratory for Condensed Matter Physics, Institute of Physics.

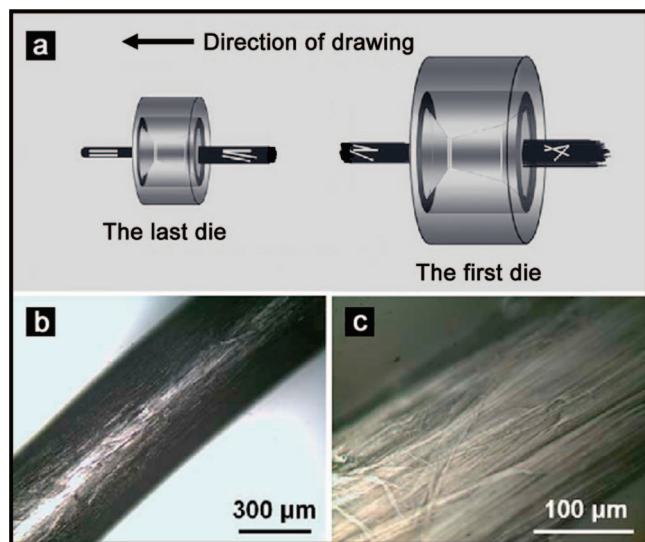


**Figure 1.** Alignment of SWNTs. (a) Schematic of the diamond wire drawing dies used to align SWNTs perfectly and densely. White bars illustrate the SWNTs alignment direction. (b) Optical image of SWNT bundle after being pulled through one diamond die with diameter of 0.55 mm. (c) Highly dense and perfectly aligned SWNTs (HDP-SWNTs) after being pulled through the last diamond die with diameter of 0.2 mm. The sample has metallic luster.

After growing for about 6 h, large-sale SWNT films can be carefully peeled off the inside wall of the quartz tube with a hook. During this removal process no obvious level of orientation is found (see Supporting Information, Figure S2). In order to align the SWNTs, a series of diamond wire drawing dies were used. The drawing was carried out through the diamond dies with decreasing pore diameters in sequence (18 dies in total ranging from 1.2 to 0.2 mm) (see Supporting Information, Figure S3 and video S1). Before being drawn, the as-grown nanotubes looked black. During each drawing, the SWNTs formed a bundle with the same diameter as that of the die used. Finally, the SWNTs became gray with metallic luster as shown in Figure 1 (see Supporting Information, Figure S4).

Panels a and b of Figure 2 show high and low magnification scanning electron microscopy (SEM) images of the SWNT bundles, respectively. It can be seen that the SWNTs fabricated in this way are perfectly aligned and highly densely packed. The width of the well-aligned SWNTs areas is roughly several micrometers. A few white dots shown in Figure 2a are traces of iron catalysts. In addition, individual bundles of SWNTs with diameters of several micrometers can be observed. For instance, bundles with diameter of 2.2 and 3.5  $\mu\text{m}$  are shown in the left and right parts of Figure 2b, respectively. These bundles are composed of dense SWNTs, and the good flexibility of SWNTs can be clearly observed at the end of the left bundle. Diameters of bundles in this work are about 2 orders of magnitude larger than those reported in refs 8 and 9. Accordingly, the number of SWNTs in each bundle is estimated to be as high as  $10^6$  about 4 orders of magnitude higher. High-resolution transmission electron microscopy (HRTEM) also reveals the as-fabricated SWNTs have a perfectly aligned microstructure as shown

in Figure 2c. It should be noted that these SWNT materials are very clean, free of amorphous carbon.

In order to characterize the structure of these HDP-SWNTs materials, several aligned SWNT bundles were put together and pressed into a rectangular piece under a pressure of 10 MPa then annealed at 400  $^{\circ}\text{C}$  for 5 min for XRD measurements. XRD data were recorded on a Rigaku D/max 2500 diffractometer with Cu  $K\alpha$  radiation ( $\lambda = 1.5406 \text{ \AA}$ ) of 40 kV and 250 mA and a step width of  $0.02^{\circ}$ .

The XRD pattern of these HDP-SWNTs exhibits significant difference compared to that of the as-grown SWNTs (see Supporting Information, Figure S5). Figure 3 shows the XRD data of these HDP-SWNTs after subtracting the background. At low angles of the XRD pattern, a strong and discrete peak appears at  $2\theta = 5.20^{\circ}$ . This Bragg peak can be indexed to (10) diffraction ( $d_{(10)}$ -spacing of 16.97  $\text{\AA}$ ) based on a two-dimensional triangular lattice of SWNTs.<sup>8,9,16–19</sup> Therefore, the lattice constant,  $a = 19.62 \text{ \AA}$ , is obtained by the equation  $a\sqrt{3}/2 = d_{(10)}$ -spacing. The following four relatively broad peaks can be indexed as (11), (20), (30), and (40), respectively. These peaks marked by arrows in Figure 3 are listed and indexed in Table 1. Assuming there are no azimuthal correlations between SWNTs within the HDP-SWNTs, we can calculate the XRD patterns by employing a homogeneous charged cylinder model for individual tubes,<sup>9,18</sup> which are closely packed into a triangular lattice (inset of Figure 3). This calculation permits us to simulate the positions, shapes, and intensities of these five peaks. By fitting the experimental data with cylindrical Bessel function  $J_0(QR)$ <sup>9,18,20</sup> (middle one in the inset of Figure 3, for a peak broadening of  $0.2^{\circ}$ ), the tube diameter ( $2R$ ) is determined to be 16.30  $\text{\AA}$  with an uncertainty of  $\pm 0.05 \text{ \AA}$ .

An interesting and important feature in the XRD pattern is that we observe a very sharp and strong peak at  $2\theta = 26.3^{\circ}$ . This peak corresponds to a  $d$ -spacing of 3.39  $\text{\AA}$ , which is usually found in graphite or multiwalled carbon nanotubes ( $d_{(002)} = 3.4 \text{ \AA}$ ).<sup>8,9</sup> In the cases of Journet et al.<sup>8</sup> and Thess et al.,<sup>9</sup> although a similar peak is observed, it is so weak that it was attributed to the remaining graphite particle introduced during the arc discharge or laser ablation. In contrast, Futaba et al. also found a similar but very broad peak, whose broadness arises from the imperfect long-range order of the SWNT sample with an average intertube spacing of 9  $\text{\AA}$ .<sup>11</sup>

However, the very sharp and strong peak at  $2\theta = 26.3^{\circ}$  in the present work, corresponding to a  $d$ -spacing of 3.39  $\text{\AA}$ , is believed to arise from the nearly ideal graphitic packing of SWNTs due to van der Waals interaction. In our case, the presence of graphite particles and/or multiwalled carbon nanotubes (MWNTs) can be excluded based on the following three reasons. First, from TEM images (see Figure 2 and Figure S6), it can be seen that our sample is nearly free of graphitic particles, even in a large area of  $\sim 8 \mu\text{m} \times 8 \mu\text{m}$ . Second, XRD data of the as-grown SWNTs (see Figure S5) also reveal the absence of the graphitic particles and/or MWNTs, because no obvious (002) peak is observed in the XRD pattern. Third, previous works<sup>15,21–23</sup> have demonstrated that the SWNTs prepared by CVD method are nearly free of graphitic particles and MWNTs. This CVD growth method

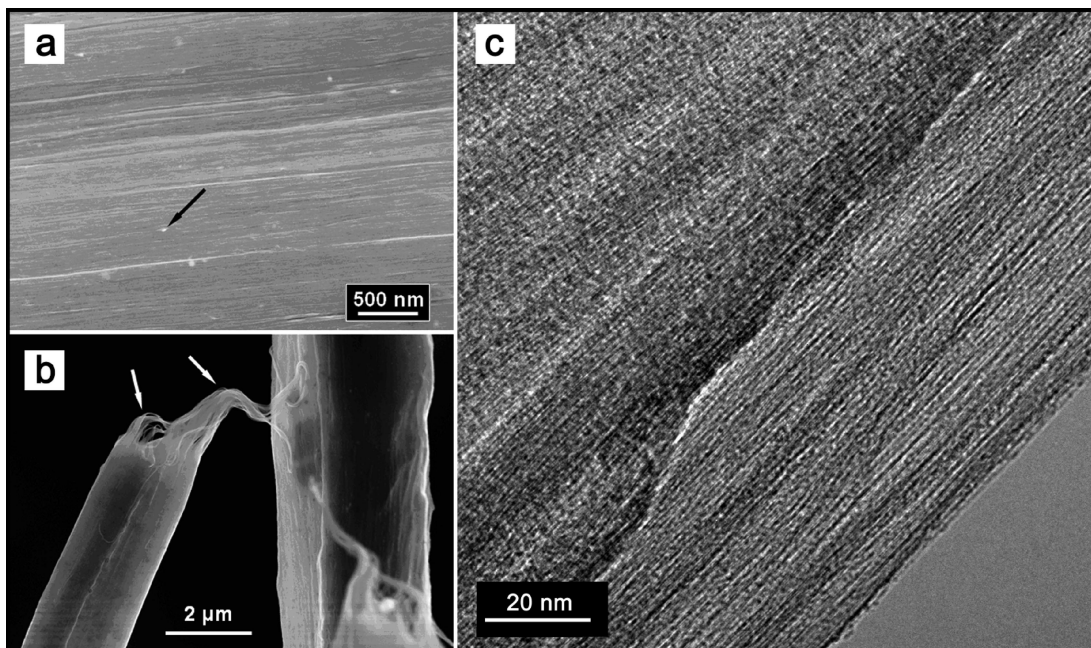


**Figure 2.** (a) High-magnification SEM image of the HDPA-SWNTs. The white dots are traces of catalyst of iron as indicated by arrows. (b) SEM image of two bundles of HDPA-SWNTs, the good flexibility of SWNTs is shown by the white arrows. (c) HRTEM image of the HDPA-SWNTs.

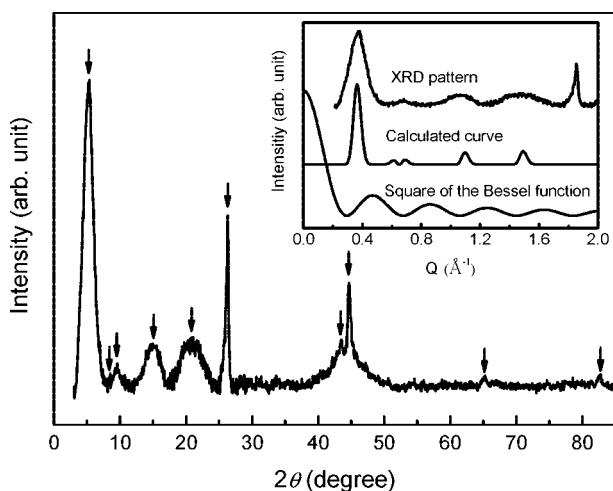


**Figure 3.** XRD patterns of the HDPA-SWNTs after subtraction of the quartz glass background (the inset of Figure S5). The inset shows the XRD pattern at low angle and the corresponding simulation by the cylindrical Bessel function  $J_0(QR)$ , where wave vector  $Q = 4\pi \sin \theta/\lambda$ , and  $R$  is the radius of the SWNT. Here the nanotube was considered as a homogeneous charged cylinder (cylinder with uniform charge distribution, regardless of the hexagonal lattice). Then the cylindrical Bessel function  $J_0(QR)$  is employed to calculate the intensities, positions, and shapes of the XRD peaks. The calculated profile is the lattice packing function after multiplying by the Bessel function. By comparison with the experimental XRD pattern, the most optimized lattice constant ( $a = 19.62 \text{ \AA}$ ) and tube radius ( $R = 8.15 \text{ \AA}$ ) can be obtained. The calculated tube radius ( $R = 8.15 \text{ \AA}$ ) is well consistent with that deduced from the experimental XRD results and that of the most probable diameter from AFM results (Figure S1).

is very different from that of Journet<sup>8</sup> and Thess.<sup>9</sup> So this strong and sharp peak at  $2\theta = 26.3^\circ$  comes indeed from the HDPA-SWNTs themselves. Moreover, the intertube spacing ( $d$ -spacing) can be figured out by  $d$ -spacing =  $a - D$ , where

**Table 1.** Indexes of the XRD Pattern of the HDPA-SWNTs<sup>a</sup>

peaks	$2\theta$ (deg)	$Q$ ( $\text{\AA}^{-1}$ )	$d_{\text{exp}}$ ( $\text{\AA}$ )	index	note
1	5.20	0.370	16.97	(10) <sup>b</sup>	HDPA-SWNTs
2	8.40	0.597	10.52	(11) <sup>b</sup>	HDPA-SWNTs
3	9.47	0.673	9.33	(20) <sup>b</sup>	HDPA-SWNTs
4	14.90	1.058	5.94	(30) <sup>b</sup>	HDPA-SWNTs
5	20.84	1.475	4.26	(40) <sup>b</sup>	HDPA-SWNTs
6	26.28	1.854	3.39	(002) <sup>c</sup>	HDPA-SWNTs
7	43.42	3.017	2.08	(100)	SWNTs
8	44.62	3.097	2.03	(110)	Fe (catalyst)
9	65.04	4.385	1.43	(200)	Fe (catalyst)
10	82.64	5.386	1.17	(211)	Fe (catalyst)

<sup>a</sup> Wave vector  $Q = 4\pi \sin \theta/\lambda$ ,  $d_{\text{exp}} = 2\pi/Q$ . Peak (100) originates from the graphene nature of SWNTs. The last three peaks are indexed to those of the catalyst iron used in our experiment. <sup>b</sup> Represents the diffraction of a two-dimensional triangular lattice. <sup>c</sup> Represents the diffraction of intertube spacing in the HDPA-SWNTs.

$a$  is the lattice constant of  $19.62 \text{ \AA}$  and  $D$  is the average diameter of the SWNTs.  $D$  ( $16.0 \text{ \AA}$ ) can be derived either from the AFM measurements (see Supporting Information, Figure S1) or by fitting the XRD data with  $J_0(QR)$  as discussed above. Thus, the calculated  $d$ -spacing is  $3.62$  and  $3.32 \text{ \AA}$ , respectively, which are close to  $3.39 \text{ \AA}$  obtained from the XRD measurement. Therefore, we conclude that the peak at  $2\theta = 26.3^\circ$  originates from the relatively uniform intertube spacing of the HDPA-SWNTs, which is very different from the SWNT solid.<sup>11</sup> For simplicity and clarity, we call this peak (002) although its origin is quite different from that of graphite or multiwalled carbon nanotubes. The intertube spacing of  $3.39 \text{ \AA}$  in this study also agrees well with the theoretical value of  $3.42 \text{ \AA}$  in a carbon nanotube crystal predicted by Tersoff et al.<sup>7</sup> based on van de Waals interaction. In addition, it is close to the experimental average value of  $3.44 \text{ \AA}$  in the  $C_{60}$  crystal.<sup>24</sup>

Supposing that the triangular packing SWNTs are composed of SWNTs with identical diameter ( $2R$ ), we can

**Table 2.** Calculated Density of Ideally Packed SWNTs with Nanotube Radius of  $\sim 8.15$  Å

CNT	$R$ (Å)	$T_{\text{SWNT}}$ (Å)	$N_{\text{SWNT}}$	$\rho_T$ (g/cm <sup>3</sup> )
(17,6)	8.10	88.15	1708	1.16
(19,3)	8.10	88.15	1708	1.16
(12,12)	8.15	2.46	48	1.16
(13,11)	8.16	88.77	1732	1.16
(14,10)	8.19	44.54	872	1.17

estimate the theoretical density ( $\rho_T$ ) with the lattice constant 19.62 Å by the following formula:

$$\rho_T = \frac{M_c N_{\text{SWNT}}}{S_{\text{lattice}} T_{\text{SWNT}}} \quad (1)$$

where  $M_c$  1.993  $\times 10^{-26}$  kg is the carbon atomic mass,  $N_{\text{SWNT}}$  the atoms in one unit cell for a single SWNT,  $S_{\text{lattice}}$  the area of the triangular lattice,  $T_{\text{SWNT}}$  the length of the unit cell along the tube axis. In Table 2, we list the possible SWNTs with different radius  $\sim 8.15$  Å (C–C, 1.422 Å), and the corresponding theoretical density.  $\rho_T$  is estimated to be  $\sim 1.16$  g/cm<sup>3</sup>. The actual density ( $\rho_T$ ) of the HDPA-SWNTs can be obtained by directly measuring the size and mass of the sample, respectively. The typical dimension of an experimental sample is  $\sim 8.80$  mm  $\times$  4.50 mm  $\times$  0.06 mm with a mass of  $\sim 2.60$  mg, and  $\rho_T$  is estimated to be  $\sim 1.09$  g/cm<sup>3</sup>, representing  $\sim 94\%$  ideal packing. If this material was put into water, you will find it sinks quickly (see Supporting Information, video S2).

The HDPA-SWNTs and the as-grown SWNTs were characterized by micro-Raman spectroscopy (Renishaw inVia Raman spectroscope). The wavelengths of the excitation laser were 632.8 nm (1.96 eV) and 514.5 nm (2.41 eV), respectively. The laser spot size is  $\sim 2$   $\mu$ m. Figure 4 shows the Raman spectra of the as-grown SWNTs and the HDPA-SWNTs collected using 632.8 nm excitation line with the laser power of  $\sim 1$  mW. Interestingly, the RBM of the HDPA-SWNTs change significantly in comparison with the as-grown SWNTs, which is in sharp contrast to almost identical Raman spectra between the SWNT forest and SWNT solid.<sup>11</sup> The RBM signals for larger diameters SWNTs in the HDPA-SWNTs are suppressed. This suppression may result from the stronger coupling between the neighboring SWNTs in the HDPA-SWNTs, which is caused by smaller intertube spacing of 3.39 Å than 9 Å in the SWNT solid.<sup>11</sup> Similar RBM suppression is also observed in the Raman spectra measured with 514.5 nm laser excitation (see Supporting Information, Figure S7).

Figure 5 shows the photoresponse of the HDPA-SWNTs measured in a vacuum of  $10^{-3}$  Pa. The outmost two electrodes serve as the source and drain electrode, respectively (inset of Figure 5). In order to eliminate the Joule heating effect, a small voltage bias of 10  $\mu$ V was applied to the sample, and the background current was  $\sim 10$   $\mu$ A. Once the HDPA-SWNTs was illuminated by a camera flash with a ultraviolet (UV) filter, the current changes from 10  $\mu$ A to  $-290$   $\mu$ A. Compared with other forms of SWNTs, such as films,<sup>25</sup> sheets,<sup>26</sup> and filaments,<sup>27</sup> the HDPA-SWNTs have a relatively large photoresponse as they are illuminated. The possible reason should be attributed to the perfectly aligned SWNTs structure, as discovered in the SWNT bundles.<sup>28</sup> In addition, the HDPA-SWNTs are expected to exhibit excellent

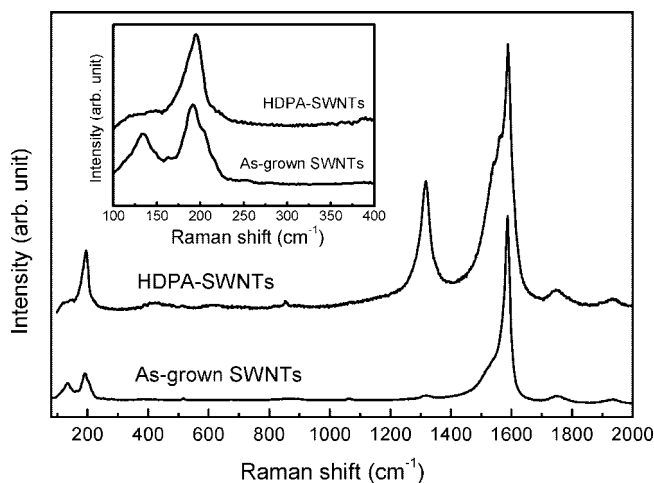


**Figure 4.** Raman spectra of the as-grown SWNTs and the HDPA-SWNTs. The wavelength of the excitation laser was 632.8 nm.

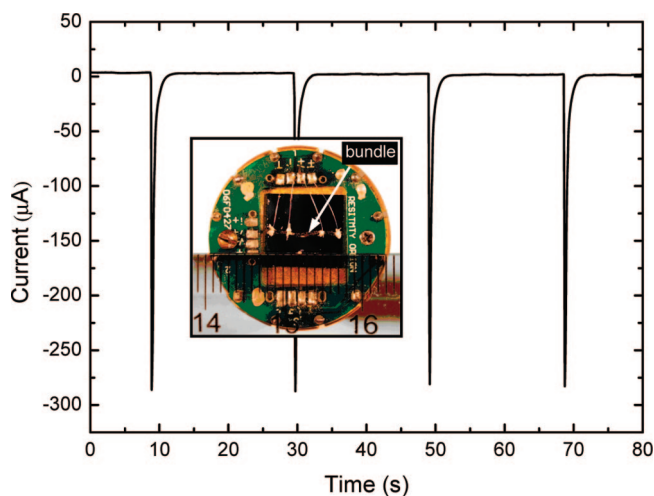


**Figure 5.** Photoresponse of the HDPA-SWNTs measured in a vacuum of  $10^{-3}$  Pa illuminated with a camera flash. The inset shows the optical image of the studied device.

electrical properties. The room-temperature resistivity of the HDPA-SWNTs is estimated to be  $\sim 2$  m $\Omega$  cm measured by a four-probe technique (inset of Figure 5), which is close to that of graphite (0.3 m $\Omega$  cm) and SWNTs crystalline ropes.<sup>9</sup> This may permit us to study the doping effect on SWNTs<sup>7,29,30</sup> in the future, such as in graphite<sup>31,32</sup> and C<sub>60</sub>.<sup>33,34</sup>

In summary, we have demonstrated a new method using a series of diamond wire drawing dies to align and pack SWNTs. SEM and TEM show that these SWNTs are highly dense and perfectly aligned. The XRD patterns of these SWNT materials are characterized with two groups of diffractions: group one is the two-dimensional triangular lattice indexed with (10), (11) etc., and the other is the (002) diffraction. Raman spectra reveal that the RBM of SWNTs with larger diameter in the HDPA-SWNTs is suppressed compared with that of the as-grown SWNTs. The perfectly aligned and highly dense SWNTs are sensitive to light illumination.

**Acknowledgment.** This work is supported by the “100 Talents Program”, Knowledge Innovation Program of Chi-

nese Academy of Sciences, “973” Program of Ministry of Science and Technology (Grant No. 2006CB932402), and National Science Foundation of China. We thank Professor Weiya Zhou and Ms. Chaoying Wang for discussion.

**Supporting Information Available:** Information and figures regarding average diameter of the individual SWNT in the HDPa-SWNTs, removal of SWNT films from the quartz tube, diamond wire dies used to fabricate HDPa-SWNTs, distinction between as-grown SWNTs and HDPa-SWNTs, raw XRD data of the HDPa-SWNTs and the as-grown SWNTs, TEM observation, and Raman spectra of the as-grown SWNTs and the HDPa-SWNTs, and two videos showing the drawing process of SWNTs using diamond wire dies and a demonstration of the large density of HDPa-SWNTs. This material is available free of charge via the Internet at <http://pubs.acs.org>.

## References

- (1) Iijima, S.; Ichihashi, T. *Nature* **1993**, *363*, 603.
- (2) Kroto, H. W.; Heath, J. R.; O'Brien, S. C.; Curl, R. F.; Smalley, R. E. *Nature* **1985**, *318*, 162.
- (3) Krätschmer, W.; Lamb, L. D.; Fostiropoulos, K.; Huffman, D. R. *Nature* **1990**, *347*, 354.
- (4) Hebard, A. F.; Rosseinsky, M. J.; Haddon, R. C.; Murphy, D. W.; Glarum, S. H.; Palstra, T. T. M.; Ramirez, A. P.; Kortan, A. R. *Nature* **1991**, *350*, 600.
- (5) Iijima, S. *Nature* **1991**, *354*, 56.
- (6) Delaney, P.; Choi, H. J.; Ihm, J.; Louie, S. G.; Cohen, M. L. *Nature* **1998**, *391*, 466.
- (7) Tersoff, J.; Ruoff, R. S. *Phys. Rev. Lett.* **1994**, *73*, 676.
- (8) Journet, C.; Maser, W. K.; Bernier, P.; Loiseau, A.; Chappelle, M. L.; Lefrant, S.; Deniard, P.; Lee, R.; Fischer, J. E. *Nature* **1997**, *388*, 756.
- (9) Thess, A.; Lee, R.; Nikolaev, P.; Dai, H.; Petit, P.; Robert, J.; Xu, C.; Lee, Y. H.; Kim, S. G.; Rinzler, A. G.; Colbert, D. T.; Scuseria, G. E.; Tománek, D.; Fisher, J. E.; Smalley, R. E. *Science* **1996**, *273*, 483.
- (10) Cheng, H. M.; Li, F.; Su, G.; Pan, H. Y.; He, L. L.; Sun, X.; Dresselhaus, M. S. *Appl. Phys. Lett.* **1998**, *72*, 3282.
- (11) Futaba, D. N.; Hata, K.; Yamada, T.; Hiraoka, T.; Hayamizu, Y.; Kakudate, Y.; Tanaike, O.; Hatori, H.; Yumura, M.; Iijima, S. *Nat. Mater.* **2006**, *5*, 987.
- (12) Hata, K.; Futaba, D. N.; Mizuno, K.; Namai, T.; Yumura, M.; Iijima, S. *Science* **2004**, *306*, 1362.
- (13) Motta, M.; Moissala, A.; Kinloch, I. A.; Windle, A. H. *Adv. Mater.* **2007**, *19*, 3721.
- (14) Li, Y.; Kinloch, I. A.; Windle, A. H. *Science* **2004**, *304*, 276.
- (15) Song, L.; Ci, L.; Lv, L.; Zhou, Z.; Yan, X.; Liu, D.; Yuan, H.; Gao, Y.; Wang, J.; Liu, L.; Zhao, X.; Zhang, Z.; Dou, X.; Zhou, W.; Wang, G.; Wang, C.; Xie, S. *Adv. Mater.* **2004**, *16*, 1529.
- (16) Ericson, L. M.; Fan, H.; Peng, H.; Davis, V. A.; Zhou, W.; Sulpizio, J.; Wang, Y.; Booker, R.; Vavro, J.; Guthy, C.; Parra-Vasquez, A. N. G.; Kim, M. J.; Ramesh, S.; Saini, R. K.; Kittrell, C.; Lavin, G.; Schmidt, H.; Adams, W. W.; Billups, W. E.; Pasquali, M.; Hwang, W.; Hauge, R. H.; Fischer, J. E.; Smalley, R. E. *Science* **2004**, *305*, 1447.
- (17) Tang, J.; Qin, L.; Sasaki, T.; Yudasaka, M.; Matsushita, A.; Iijima, S. *Phys. Rev. Lett.* **2000**, *85*, 1887.
- (18) Maniwa, Y.; Matsuda, K.; Kyakuno, H.; Ogasawara, S.; Hibi, T.; Kadowaki, H.; Suzuki, S.; Achiba, Y.; Kataura, H. *Nat. Mater.* **2007**, *6*, 135.
- (19) Grigorian, L.; Williams, K. A.; Fang, S.; Sumanasekera, G. U.; Loper, A. L.; Dickey, E. C.; Pennycook, S. J.; Eklund, P. C. *Phys. Rev. Lett.* **1998**, *80*, 5560.
- (20) Fujiwara, A.; Ishii, K.; Suematsu, H.; Kataura, H.; Maniwa, Y.; Suzuki, S.; Achiba, Y. *Chem. Phys. Lett.* **2001**, *336*, 205.
- (21) Cassell, A. M.; Raymakers, J. A.; Kong, J.; Dai, H. *J. Phys. Chem. B* **1999**, *103*, 6484.
- (22) Hafner, J. H.; Bronikowski, M. J.; Azamian, R. B.; Nikolaev, P.; Rinzler, A. G.; Colbert, D. T.; Smith, K. A.; Smalley, R. E. *Chem. Phys. Lett.* **1998**, *296*, 195.
- (23) Lyu, S. C.; Liu, B. C.; Lee, S. H.; Park, C. Y.; Kang, H. K.; Yang, C. W.; Lee, C. J. *J. Phys. Chem. B* **2004**, *108*, 1613.
- (24) David, W. I. F.; Ibberson, R. M.; Matthewman, J. C.; Prassides, K.; Dennis, T. J. S.; Hare, J. P.; Kroto, H. W.; Taylor, R.; Walton, R. M. *Nature* **1991**, *353*, 147.
- (25) Lien, D. H.; Hsu, W. K.; Zan, H. W.; Tai, N. H.; Tsai, C. H. *Adv. Mater.* **2006**, *18*, 98.
- (26) Lu, S. X.; Panchapakesan, B. *Nanotechnology* **2006**, *17*, 1843.
- (27) Zhang, Y.; Iijima, S. *Phys. Rev. Lett.* **1999**, *82*, 3472.
- (28) Liu, G. T.; Liu, Z.; Zhao, Y. C.; Zheng, K. H.; Huang, H. B.; Ma, W. J.; Gu, C. Z.; Sun, L. F.; Xie, S. S. *J. Phys. D: Appl. Phys.* **2007**, *40*, 6898.
- (29) Lee, R. S.; Kim, H. J.; Fischer, J. E.; Thess, A.; Smalley, R. E. *Nature* **1997**, *388*, 255.
- (30) Tang, Z. K.; Zhang, L.; Wang, N.; Zhang, X. X.; Wen, G. H.; Li, G. D.; Wang, J. N.; Chan, C. T.; Sheng, P. *Science* **2001**, *292*, 2462.
- (31) Dresselhaus, M. S.; Dresselhaus, G. *Adv. Phys.* **1981**, *30*, 139.
- (32) Weller, T. E.; Ellerby, M.; Saxena, S. S.; Smith, R. P.; Skipper, N. T. *Nat. Phys.* **2005**, *1*, 39.
- (33) Fleming, R. M.; Ramirez, A. P.; Rosseinsky, M. J.; Murphy, D. W.; Haddon, R. C.; Zahurak, S. M.; Makhija, A. V. *Nature* **1991**, *352*, 787.
- (34) Zhou, O.; Zhu, Q.; Fischer, J. E.; Coustel, N.; Vaughan, G. B. M.; Heiney, P. A.; Mccauley, J. P., Jr.; Smith, A. B., III. *Science* **1992**, *255*, 833.

NL073007O